Citation information: DOI 10.1109/TMECH.2022.3183576, IEEE Transactions on Mechatronics

An All-Soft Variable Impedance Actuator Enabled by Embedded Layer Jamming

Brian H. Do[1], Inrak Choi[2], and Sean Follmer[1]

***Abstract*—Biological muscle is a multi-functional actuator capable of varying its stiffness and damping. The design of similarly multipurpose variable impedance actuators has benefits for improving physical robot interaction, such as by enabling variable impedance manipulators with more capability and greater safety. We present the concept for a soft jamming brake and artificial muscle (SJBAM). By incorporating a jamming brake inside of a pneumatic artificial muscle, we achieve synergistic benefits which enable new functionalities, improve muscle static and dynamic response, and expand the brake's capabilities. The SJBAM can store elastic energy like a pneumatic artificial muscle and also act as a brake or clutch. By independently controlling the muscle and brake pressures, we can vary the SJBAM's stiffness and damping. We derive models for this actuation concept and examine the performance of the SJBAM both theoretically and experimentally. Additionally, we present open- and closed-loop position control demonstrations with a 1-degree-of-freedom manipulator actuated by an antagonistic pair of SJBAMs.**

***Index Terms*—Variable impedance actuators (VIAs), soft robotics, layer jamming, variable stiffness, variable damping.**

I. Introduction

WHEN comparing current robotic actuators to their biological counterparts, one key distinguishing feature of muscle is its ability to vary both stiffness and damping. Biological muscle is versatile, and can behave like a brake, a strut, and a spring in addition to a motor [1]. Animals vary their muscle impedance depending on the application. For example, legged animals use variable damping to stabilize their walking gait [2] and vary their leg stiffness during running [3].

Variable impedance actuators (VIAs) have the potential to enable more robust, dexterous, and safe interactions between robots and the outside world. Although traditional robotic actuators can be programmed to alter their interaction impedances, varying impedance mechanically allows robots to achieve adaptive behavior without the same stability and bandwidth limitations inherent to active control – enabling physically embodied intelligence [4].

VIAs are defined by their ability to deviate from an equilibrium position due to their effective stiffness, damping, and/or inertia [4]. One subclass of VIAs are variable stiffness actuators (VSAs). While variable stiffness can improve intrinsic safety, it can also introduce new challenges, such as underdamped dynamics, and may result in instability [5]. Inherent joint compliance from VSAs can also make unexpected collisions more dangerous in a pre-tensioned state or at high velocities due to their energy storage [6]. Another subclass of VIAs are variable damping actuators (VDAs). VDAs enable new capabilities such as energy dissipation and address limitations of compliance alone, such as improving position accuracy by minimizing structural resonances. Despite this, they have received comparatively less attention to VSAs [7].

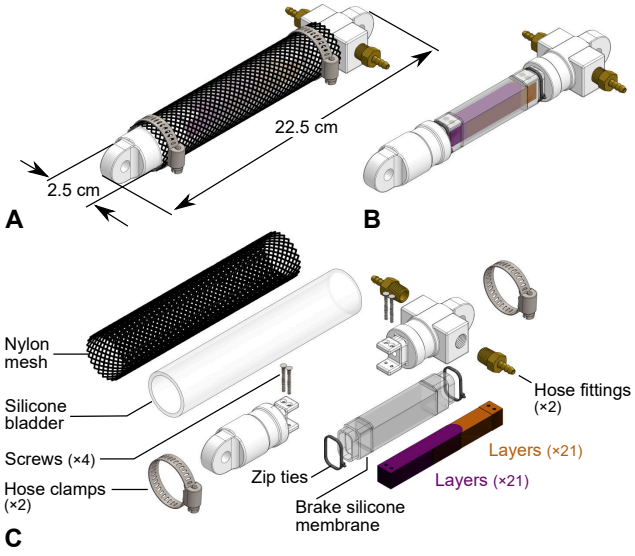

Fig. 1. Schematic of an SJBAM and its constituent components (A) The SJBAM consists of an outer McKibben muscle and (B) an inner layer jamming brake. (C) SJBAM exploded view. The outer McKibben muscle is composed of a nylon mesh surrounding a silicone elastomeric bladder secured to end caps using hose clamps. Inside is a layer jamming brake consisting of a silicone membrane and two sets of 42 interdigitated PTFE layers, each mounted to an end cap using 2 screws. Zip ties secure the membrane to the end caps. Air is delivered independently to the muscle and brake via hose fittings.

Beyond variable impedance, muscle also has high power-to-weight ratio and is soft. Compliance can be built into robotic actuators in several ways, such as by incorporating springs [4] or by using soft materials [8]. Actuators made out of inherently compliant and flexible materials with properties analogous to biological muscle, such as pneumatic artificial muscles (PAMs), can enable the creation of entirely soft robots [8].

While there has been significant interest in VIAs and in soft actuators, there has not been an all-soft VIA with both controllable variable stiffness and damping. Such all-soft VIAs could enhance the embodied intelligence of soft robots, enabling wider forms of interactions. Traditional robots could also benefit from all-soft VIAs by incorporating them alongside

[1]Department of Mechanical Engineering, Stanford University, Stanford, CA 94305 USA. (email: brianhdo@stanford.edu; sfollmer@stanford.edu)

[2] Department of Mechanical Engineering, Seoul National University, Seoul 08826, Republic of Korea. (email: irchoi@snu.ac.kr)

This work is supported in part by the National Science Foundation Graduate Research Fellowship Program. Part of this work was performed at the Stanford Nano Shared Facilities (SNSF), supported by the National Science Foundation under award ECCS-1542152.

Citation information: DOI 10.1109/TMECH.2022.3183576, IEEE Transactions on Mechatronics

traditional motors in a macro-mini actuation approach [9].

We propose a novel low-cost, all-soft VIA composed of a soft jamming brake and artificial muscle (SJBAM) (Fig. 1). The SJBAM incorporates a soft layer jamming brake (SLJB) inside of a PAM. The SJBAM's mechanical design enables independent control of its stiffness and damping. The SJBAM can store elastic energy like a PAM or dissipate energy like a brake. The SJBAM can vary its damping and inertial properties, enabling it to act as a clutch or strut. The combination of an SLJB and a PAM also yields three main synergistic benefits: 1) layer jamming with super-atmospheric pressure ranges and without the need for negative pressure, 2) increased muscle force production, and 3) improved response time. Overall, the SJBAM addresses several limitations of PAMs while retaining low inertia, high force density, and inherent compliance.

In this paper we explore the design, modeling, and empirical evaluation of the SJBAM. Section II discusses related work. Section III introduces the concept for and our implementation of the SJBAM. We derive its quasi-static and stiffness models in Section IV and validate these models with quasi-static and dynamic tests in Sections V and VI. We present open- and closed-loop position control demonstrations using a 1-degree-of-freedom (DOF) manipulator comprised of an antagonistic pair of SJBAMs in Section VII. Section VIII discusses general principles to maximize benefits of the SJBAM.

II. Related Work

A. Variable Stiffness Actuators and Soft Actuators

VSAs are a major focus of the robotics community [4]. A multitude of designs have been proposed and can be broadly divided into those that vary spring preload, transmission between load and spring, and the spring's physical properties [4]. The focus on VSAs has been driven by the desire for safer and more robust actuators. These goals also motivated the parallel development of soft robots made of low stiffness materials [8].

A core challenge in soft robotics today is controllable variable stiffness [10]. However, unlike traditional actuators which must increase compliance, soft actuators – which are inherently compliant – must increase stiffness. Fundamental questions remain about simultaneously achieving variable stiffness, integrating designs into entirely soft robot bodies, and optimizing interactions with the environment. Variable stiffness could enable soft robots to better reject disturbances and improve their precision.

One of the most widely used soft actuators is the PAM [8], [11]. PAMs passively behave as nonlinear springs and when used in an antagonistic architecture can provide variable joint stiffness. PAMs have a number of attractive properties, including intrinsic compliance, low weight, easy fabrication, and high force density. The most widely used PAM is the McKibben muscle [12], which is composed of an elastomer bladder inside of a flexible, inextensible fiber mesh which converts radial expansion when pressurized into axial motion [13].

Using PAMs as VSAs introduces tradeoffs such as the inability to produce a high stiffness system with little yielding around its equilibrium point [14]. Furthermore, maintaining an equilibrium position requires a preload, which may generate large forces on the surrounding structure [14].

Prior work to enable stiffness control of PAMs includes parallel arrangements of extensor and contractor muscles [15], which further complicates position control due to interaction forces between the muscles; pneumatic-hydraulic actuation, which requires a vertical muscle orientation to prevent mixing of hydraulic fluid with pneumatics [16]; and embedded tendons [17], which require motors to control the tendon tension.

B. Variable Damping Actuators

Biological muscle has variable damping [18], [19]. Organisms can alter the damping of their joints [20] and entire body segments [19] to produce stable locomotion patterns. Without varying damping, actuators are limited in their ability to match the performance and versatility of biological muscle.

Despite comparatively less focus on variable damping than variable stiffness, energy-dissipative elements such as brakes or dampers can improve robot safety and broaden impedance. They are classified as passive, semi-active, or active, depending on the energy required to operate them. Passive dampers have fixed damping, which may lower potential performance due to energy loss. Klute et al. used a passive hydraulic damper in parallel with a McKibben muscle to absorb excess energy after collisions [18]. Semi-active damping enables a range of damping while retaining stability guarantees due to removal of energy from a system. Laffranchi et al. developed a variable physical damping actuator using a friction disk damper actuated by stacked piezo-electric actuators [5]. Finally, active damping involves an active force element which can overcome the passive system dynamics, which can destabilize the system.

Several approaches combining a PAM and a brake for hybrid actuation have been investigated, including using a magnetorheological brake [21], an electrorheological damper [22], and a motor with a magnetic particle brake [9]. These approaches are limited by their low force density, introduce rigid components into otherwise soft actuators, increase system size, and need to expend energy to maintain braking force.

C. Jamming

Jamming represents an intersection of variable stiffness and damping devices. It involves compacting layers/particles together via a pressure gradient. Prior jamming work has focused on using a negative pressure source to produce a binary transition between soft and rigid states, allowing structures to alternate between retaining their shapes and compliantly interacting with their environment [23]–[26]. In the context of actuators, jamming has mainly been used to increase bending stiffness [27]–[29]. Recently, layer jamming has been used to precisely modify the overall mechanical characteristics of structures through controllable stiffness or damping [30], [31]. When a laminar structure is initially jammed, its layers are cohesive. When forces above a certain threshold are applied, the layers slide, resulting in energy dissipation via friction.

We previously leveraged this to produce the SLJB [31]. The SLJB relies on a negative pressure difference to compress layers together. This compression produces increased normal force on the layers and consequently, increased friction between them, resulting in a larger force required to pull the layers apart which can be tuned via the pressure difference.

Citation information: DOI 10.1109/TMECH.2022.3183576, IEEE Transactions on Mechatronics

III. Materials and Methods

A. Concept Overview

The SJBAM consists of a layer jamming brake embedded inside of a PAM. The resulting synergistic benefits are improved performance compared to a PAM in shock absorption, stiffness variation with constant load, and stiffness variation at constant position – all common VIA use cases [4].

Overall, the SLJB tunes the SJBAM's linear stiffness and damping. The brake functions as a semi-active Coulomb friction damper, with energy dissipation tuned by the pressure difference across the brake. This reduces oscillation of the inherently underdamped PAM, and unlike a viscous damper, the SLJB can produce high damping at low velocities and can clamp a mass in place. No energy is required to maintain the braking state once the pressure difference has been set. Jamming produces an orders-of-magnitude increase in the SJBAM stiffness by varying the SLJB's moment of inertia. The SLJB can be "mechanically programmed" to passively yield at a given force, allowing for energy dissipation above a threshold. Additionally, the SJBAM can reset an extended SLJB via unjamming the brake and contracting the PAM. Finally, the incorporation of a brake inside of a PAM does not increase the overall device profile, and the softness of both the brake and muscle in the SBJAM's passive state enables the SJBAM to be used in applications where softness is advantageous, such as in human-robot interaction.

This structure results in several benefits for the SLJB. Traditional jamming devices have been restricted to a maximum pressure difference of 1 atm, thus limiting the maximum force they can produce, and have required the use of a vacuum source to generate that pressure difference relative to the atmosphere. Incorporating a jamming brake inside of a PAM, as shown in Fig. 2, addresses these issues. Since PAMs operate at pressures >1 atm, a pressure difference ΔP across the brake can be achieved purely through pressurizing the muscle. Thus, the SJBAM can generate a pressure gradient across the brake without a vacuum source, enabling positive pressure jamming, and that pressure difference can span a super-atmospheric range, greatly increasing the braking output force.

The SJBAM structure also produces several benefits for the PAM. Besides enhanced damping, because the brake occupies a central volume which reduces the PAM interior volume, PAM inflation/deflation times are reduced, improving PAM dynamic response. This reduced volume also slightly increases muscle force output over its entire range of motion.

One key consideration is the choice of soft actuator to use with the brake. The maximum SLJB strain is 100%, with higher strains separating the two sets of layers. Thus, in the SJBAM, the brake's travel should match the actuator's displacement and the brake's minimum length should match the actuator's minimum length. The maximum brake displacement is constrained by the maximum actuator length. In theory, any fluidic actuator with a maximum strain <100% can be used.

B. Design and Fabrication

We implement the SJBAM using a pneumatic McKibben muscle due to its widespread use throughout the robotics community to enable direct comparison of the SJBAM performance against that of the McKibben muscle.

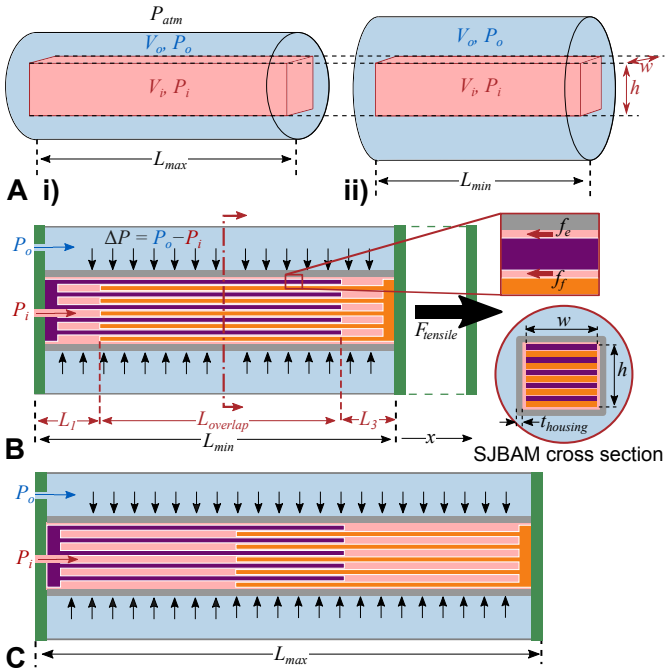

Fig. 2. SJBAM quasi-static model. (A) i) The SJBAM consists of a brake (in red) inside of a PAM (in blue). The pressures P_i and P_o in the brake and the muscle, respectively, can be controlled independently. ii) As the muscle contracts, the brake cross sectional area wh remains constant. (B) SJBAM schematic, showing a jammed state with an external applied force, F_{tensile}. F_{tensile} is opposed by the brake elastic membrane tension f_e and inter-layer friction f_f resulting from the normal force produced by the pressure differential ΔP caused by the difference in muscle pressure P_o and brake pressure P_i. The minimum SJBAM length L_{min} corresponds to the maximum amount of overlap between the layers L_{overlap}. (C) The SJBAM can be pulled to a maximum length L_{max} defined by the muscle's resting length.

The inner layer jamming brake and outer fluidic muscle of the SJBAM are both mounted to the same set of end caps. The jamming brake unit consists of n layers of stacked material evenly split into two sets of layers, each attached to an endcap. There is a length L_1 which is the length protruding from the left endcap that does not overlap with the layers from the right; a length L_{overlap} which is the length corresponding to the overlapping region between the two sets of layers; and L_3 which is the length from the right endcap that does not overlap with the layers from the left.

Fig. 1 shows a diagram of an SJBAM. The inner SLJB consists of 42 PTFE layers, a flexible silicone outer cover, 4 screws, and 2 end caps. The 42 layers are divided so that 21 layers are fixed to each end cap, with the layers laid in an interdigitated pattern. Each PTFE layer is 0.254 mm thick, 64.7 mm long, and 11.43 mm wide. PTFE was chosen as the layer material due to its relatively low stick-slip motion [31]. We cut the layers using a CO_2 laser cutter.

The flexible outer cover of the SLJB is made from Ecoflex 5 platinum catalyzed silicone (Smooth On, Inc.). This silicone cover was created by injection molding using a dispenser which mixed the two-part silicone cure into a mold created using an Objet24 3D printer (Stratasys, Ltd.). The cover has a wall thickness of 1 mm. The inclusion of a layer jamming

Citation information: DOI 10.1109/TMECH.2022.3183576, IEEE Transactions on Mechatronics

brake results in a total weight of 169 g for the SJBAM compared to 136 g for a standalone McKibben muscle.

The McKibben muscle consists of a polyester sleeve and a silicone bladder, which was also made by injection molding in a 3D printed mold. The bladder is made from Dragon Skin 10 Medium (Smooth On, Inc.) with a wall thickness of 2.5 mm, inner diameter of 25.4 mm, and length of 150 mm.

The end caps were 3D-printed using an Objet24 and were designed for mounting on an Instron machine. One end cap has two air channels to direct air flow from an exterior air supply to either the brake or muscle. Thus, SLJB and McKibben muscle pressures can be controlled independently. Tubing is secured to the end cap by hose fittings. A pressure difference across the SLJB, and thus jamming, can be induced by setting the SLJB to a lower pressure than the surrounding McKibben muscle. Likewise, the SLJB can be unjammed by setting the SLJB to the same pressure as the surrounding McKibben muscle.

The assembly of the SJBAM is as follows: connect the brake layers to the two end caps and fasten each set down with corresponding screws. Afterwards, slide the brake cover onto one end cap and interleave the layers together, sliding the brake cover onto the opposite end cap once the layers are interdigitated. Secure the ends of the brake cover to the end caps with zip-ties. Then, slide on the muscle elastomeric bladder and braided mesh, securing them with hose clamps. Finally, screw hose fittings into the appropriate end cap.

IV. Modeling

The SJBAM has three operating modes: 1) a VIA, 2) an enhanced layer jamming brake, and 3) a McKibben muscle. In this section, we present quasi-static models for each mode and derive a model for the stiffness of an SJBAM.

A. SJBAM as a Variable Impedance Actuator

As discussed in Section III, the SJBAM is physically constructed as a layer jamming brake inside of a PAM. As a result, when the SJBAM is used as a VIA, we can model the SJBAM as a brake and muscle in parallel. Fig. 2(A) shows a diagram of this arrangement, with the brake occupying an inner volume V_i at an inner pressure P_i and the muscle occupying the remaining outer volume V_o at an outer pressure P_o. Thus, independent models for the SJBAM as a brake and the SJBAM as a muscle can be summed to form the complete model for the SJBAM as a VIA:

$$F_{\text{SJBAM,overall}} = F_{\text{SJBAM,brake}} + F_{\text{SJBAM,muscle}} \tag{1}$$

As will be shown, to function solely as a brake, we can set P_o to atmospheric pressure (0 kPa, gauge). To function solely as a muscle, we can set $P_o = P_i$. Other combinations of P_o and P_i will result in some force contribution from both the brake and muscle components of the SJBAM.

B. SJBAM as a Brake

The SJBAM can be equivalently thought of as a layer jamming brake inside of an independently-pressurized chamber. The brake behavior can be divided into two regimes: 1) a pre-slide regime before the layers start to slide and 2) a post-slide regime after the layers have begun sliding.

Fig. 2(B) shows a diagram of an axial cross section of the SJBAM. The brake itself is subject to a pressure difference $\Delta P = P_o - P_i$ across the brake membrane. The difference in pressure produces a normal force on all sides of the layer sets, resulting in friction between the layers and membrane tension which must be overcome before the layers can be pulled apart. For practical use, $P_o > P_{\text{atm}}$, while $P_o > P_i > 0$ kPa, absolute so that $\Delta P \geq 0$. If $P_i > P_o$ such that $\Delta P < 0$, the resulting "brake" force is equivalent to when $\Delta P = 0$, that is, there is no normal force on the layers and no jamming.

1) Pre-Slide Regime: If the tensile force applied to the SJBAM is less than the static friction force F_f generated by the layers, the layers remain stationary relative to each other.

In the pre-slide regime, the brake of the SJBAM acts as a stiff spring which stores mechanical energy. We modeled the SLJB as a set of springs in series. Therefore, the tensile force in the quasi-static case is:

$$F_{\text{tensile}} = k_{\text{eff}} x = (1/k_1 + 1/k_2 + 1/k_3)^{-1} x \tag{2}$$

where k_{eff} is the net effective spring constant of the layers and the stiffness of each set of layers is:

$$k_i = E_i A_i / L_i \quad (i = 1, 2, 3) \tag{3}$$

where E_i is the elastic modulus of the layer material, L_i and A_i are the length and total cross-sectional area, respectively of each layer set, and $i = 2$ refers to the overlapped layers.

In practice, the experimental k_{eff} is often much less than that predicted by (2) due to brake construction tolerances allowing the layers to move. In these cases, k_{eff} can be determined using the empirical calibration method outlined by Choi et al. [31].

2) Post-Slide Regime: Once the applied tensile force exceeds the static friction force F_f generated by the layers and the membrane tension F_e, the layers will start sliding, absorbing mechanical energy in the process. In this case, the braking force is the sum of the frictional forces F_f from the layer interfaces and the elastic membrane tension forces F_e:

$$F_{\text{SJBAM,brake}} = F_f + F_e = \sum_{1}^{n-1} f_f + \sum_{s=1}^{4} f_{e,s} \tag{4}$$

where f_f is the friction force from one layer interface and $f_{e,s}$ is the tension from one side s – top, left, right, bottom – of the brake elastic membrane. Using the results derived from [26], f_f and f_e can be written as:

$$f_f = \mu w (L_{\text{overlap}} - x) \Delta P \tag{4a}$$

and

$$f_{e,s} = \sqrt{E_e A_s \Delta P \mu_e d_s x} \tag{4b}$$

where E_e is the membrane elastic modulus, μ_e is the friction coefficient between the brake membrane and the layers, and we consider tension from each side s of the brake membrane. As Fig. 2(B) shows, each side has a rectangular interface with the layers with dimensions d_s, which is h or w, by $L_{\text{overlap}} + x$ and cross-sectional area $A_s = d_s t_{\text{housing}}$. We also consider the spring force from the layers stretching as given by (2).

C. SJBAM as a Muscle

An independent model for the SJBAM as a muscle can be derived by considering a generalized model for an ideal cylindrical PAM. The force of such an ideal PAM is [13]:

$$F = -P' \frac{dV}{dx} \tag{5}$$

where F is the force generated, P' is the pressure difference between the muscle and its ambient environment, dV is the change in volume, and dx is the axial displacement.

Consider the case where V is divided into an inner volume V_i with a fixed cross-sectional area and an outer volume V_o encompassing the remaining actuator volume. Fig. 2(A) shows an example of this. The total force produced by the actuator is the sum of the forces F_i and F_o from V_i and V_o, respectively:

$$\begin{aligned} F = F_i + F_o &= -P_i' \frac{dV_i}{dx} - P_o' \frac{dV_i}{dx} \\ &= -(P_i - P_{\text{atm}}) \frac{dV_i}{dx} - (P_o - P_{\text{atm}}) \frac{dV_o}{dx} \end{aligned} \tag{6}$$

where V_i and V_o are at internal pressures P_i, P_o producing forces F_i, F_o, respectively, and P_{atm} is atmospheric pressure.

Now, consider the case when the actuator performs work and shortens in length. When the PAM contracts, $F_i < 0$ since $\frac{dV_i}{dx} > 0$ since the cross sectional area remains constant. This tensile force corresponds to the work done by the working fluid on the end caps of the PAM. Meanwhile, $F_o > 0$ since $\frac{dV_o}{dx} < 0$ in an ideal PAM. Thus, the resultant contractile force F is less than F_o. Reducing or eliminating the inner volume V_i increases the force generated.

In the case of the SJBAM, V_i corresponds to the volume enclosed by the SLJB. Thus, V_i is a rectangular prism with length L and cross-sectional area wh. With the SLJB, nearly all of its volume is occupied by its solid layers, thus resulting in a negligible $\frac{dV_i}{dx}$ as the brake is stretched. V_o corresponds to the remaining SJBAM volume. Fig. 2(A) illustrates this. To operate the SJBAM as a McKibben muscle, the SJBAM is pressurized such that $P_i = P_o > P_{\text{atm}}$ so that $\Delta P = 0$ and by (4), $F_{\text{SJBAM, brake}} = 0$. Therefore, the force generated by the SJBAM when used as a muscle is higher than that of a traditional PAM of equivalent volume V. Specifically, the force generated by the SJBAM is equal to the force produced by an ideal PAM plus an additional force F_{offset} as a result of excluding the losses F_i:

$$F_{\text{SJBAM,muscle}} = F_{\text{PAM}} + F_{\text{offset}} = F_{\text{PAM}} + Pwh \tag{7}$$

D. SJBAM Stiffness

Because the muscle and the brake are in parallel:

$$k_{\text{SJBAM}} = k_{\text{muscle}} + k_{\text{brake}} \tag{8}$$

k_{muscle} is the stiffness for the muscle used in the SJBAM. For the device presented in this paper, k_{muscle} is the McKibben muscle stiffness; if a different muscle were used, k_{muscle} would be for that corresponding muscle type. In general, an actuator's stiffness k is the derivative of its force output F with respect to its displacement x:

$$k = \frac{dF}{dx} \tag{9}$$

In general, for an SJBAM composed of a fluidic actuator:

$$k_{\text{muscle}} = \frac{dF_{\text{SJBAM,muscle}}}{dx} = \frac{dF_{\text{PAM}}}{dx} + wh\frac{dP_o}{dx} \tag{10}$$

For the SJBAM presented in this paper, F_{PAM} is the force produced by a McKibben muscle. Due to its simplicity and widespread use in literature, we use the Chou-Hannaford model for an ideal McKibben muscle [13] in this analysis. However, any relevant model could be used for F_{PAM} as desired. Using this and $\varepsilon = 1 - \frac{L_{\min}+x}{L_{\max}}$:

$$\frac{dF_{\text{PAM}}}{dx} = \pi r_0^2[a(1-\varepsilon)^2 - b]\frac{dP_o}{dx} + \frac{2\pi r_0^2 a}{L_{\max}^2} P_o(L_{\min} + x) \tag{11}$$

As is the case with other McKibben-type muscles, $\frac{dP_o}{dx}$ is difficult to calculate for the SJBAM due to coupling between length, volume, and pressure for a closed volume of gas inside a McKibben muscle. In the case of active pressurization of the McKibben to a different pressure, $\frac{dP_o}{dx}$ becomes even more challenging to calculate due to the muscle's nonlinearity [32]. However, with an appropriate closed-loop pressure control system or a large enough external gas volume connected to the actuator, approximately constant actuator pressure is maintained throughout a contraction cycle; that is, $\frac{dP_o}{dx} = 0$. Applying this, we find that the SJBAM muscle stiffness matches that of an equivalent McKibben muscle:

$$k_{\text{muscle}} = \frac{2\pi r_0^2 a}{l_0^2} P_o(L_{\min} + x) \tag{12}$$

While a single McKibben muscle does exhibit variable stiffness, it is difficult to control that stiffness due to the difficulty in calculating $\frac{dP_o}{dx}$ when varying P_o. Thus, a single McKibben muscle lacks independent pressure and displacement control. As a result, variable stiffness applications involving McKibben muscles have mostly been restricted to the control of joint stiffness due to the need for antagonistic muscle arrangement [4].

The brake stiffness can be calculated in a similar manner. Assuming the brake is in the sliding regime and $\frac{dP_o}{dx} = 0$:

$$k_{\text{brake}} = \frac{dF_{\text{brake}}}{dx} = \frac{dF_f}{dx} + \frac{dF_e}{dx} \tag{13}$$

where:

$$\frac{dF_f}{dx} = (n-1)\mu W \left[(L_{\text{overlap}} - x)\left(-\frac{dP_i}{dx}\right) - \Delta P \right] \tag{13a}$$

$$\frac{dF_e}{dx} = \sum_{s=1}^{4} \sqrt{\frac{E_e A_s \mu_e d_s}{\Delta P x}} \left[\left(-\frac{dP_i}{dx}\right) x + \Delta P \right] \tag{13b}$$

Since $\frac{dV_i}{dx} \approx 0$, $\frac{dP_i}{dx} = \frac{dP_i}{dV_i}\frac{dV_i}{dx} \approx 0$. Thus (13) simplifies to:

$$k_{\text{brake}} = -(n-1)\mu w \Delta P + \sum_{s=1}^{4} \sqrt{\frac{E_e A_s \mu_e d_s}{x}} \sqrt{\Delta P} \tag{14}$$

Therefore, the stiffness of an SJBAM is:

$$\begin{aligned} k_{\text{SJBAM}} = &\frac{2\pi r_0^2 a}{l_0^2} P_o(L_{\min} + x) - (n-1)\mu w \Delta P \\ &+ \sum_{s=1}^{4} \sqrt{\frac{E_e A_s \mu_e d_s}{x}} \sqrt{\Delta P} \end{aligned} \tag{15}$$

Citation information: DOI 10.1109/TMECH.2022.3183576, IEEE Transactions on Mechatronics

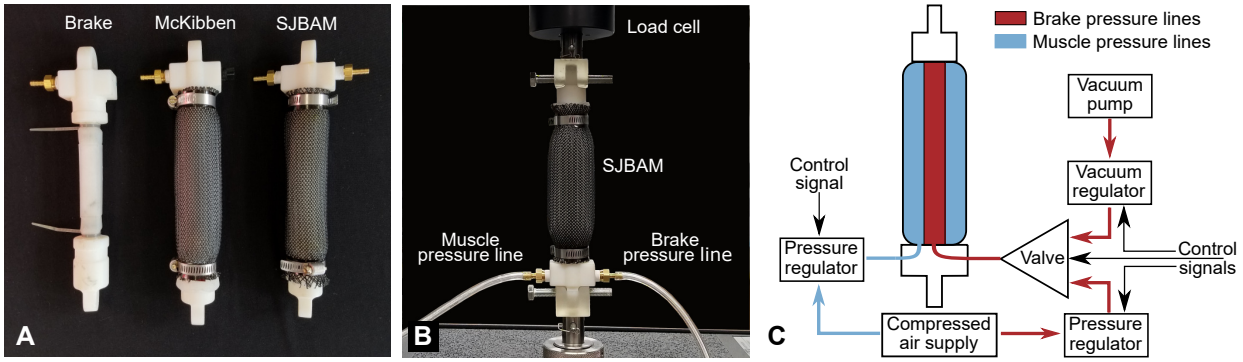

Fig. 3. Setup for quasi-static characterization of the SJBAM. (A) (From left to right) a standalone layer jamming brake, McKibben muscle, and SJBAM. (B) Quasi-static force-displacement curves were measured using an Instron 5565. (C) System architecture to control an SJBAM.

Because $\frac{dP_i}{dx} \approx 0$, we can change the inner brake pressure P_i while retaining independent control of the brake stiffness. Therefore, the overall SJBAM stiffness can be controlled by changing the brake pressure P_i to produce the required ΔP for desired actuator force at a given displacement.

V. Quasi-Static Experimental Results

A. Test Setup and Experimental Procedure

For quasi-static characterization, an SJBAM was fabricated along with a standalone McKibben muscle and standalone layer jamming brake, each with the same dimensions as that found in the SJBAM to allow for direct performance comparison (Fig. 3(A)). We performed tensile tests using an Instron 5565 with a 500 N load cell (Fig. 3(B)).

Fig. 3(C) illustrates the system architecture used to control the SJBAM. Positive pressure was regulated using a QB3 regulator (Proportion Air). Negative pressure was regulated using an MM1 regulator (Proportion Air). Throughout this paper, we report the pressure as gauge pressure.

B. SJBAM as a Muscle

1) PAM Model: While the Chou-Hannaford model's simplicity lends itself well for analysis, it has been widely reported that it can differ from empirical results by up to 15%. To aid comparison of empirical SJBAM muscle performance with the theory, we use a modified version of the Chou-Hannaford model [33]. Thus, in (7), F_{PAM} is now:

$$F_{\text{PAM}} = \kappa_F(\pi r_0^2)P[a(1-\kappa_\varepsilon\varepsilon)^2 - b] \tag{16}$$

where $a = 3/\tan^2(\alpha_0)$ and $b = 1/\sin^2(\alpha_0)$ with α_0 being the initial braid angle in the deflated muscle state. Additionally, κ_F is the force tuning parameter defined as:

$$\kappa_F(P) = \frac{F_{\text{meas,max}}(P)}{(\pi r_0^2)P(a-b)} \tag{16a}$$

and κ_ε is the strain tuning parameter defined as:

$$\kappa_\varepsilon(P) = \frac{1}{\varepsilon_{\text{meas,max}}(P)}\left(1 - \frac{1}{\sqrt{3}\cos(\alpha_0)}\right) \tag{16b}$$

We use this calibrated Chou-Hannaford model as our PAM model for comparison to capture discrepancies due to construction and material properties. By doing so, we can better determine that differences between predicted and actual SJBAM muscle behavior are due to more fundamental underlying reasons between a standalone PAM and our device.

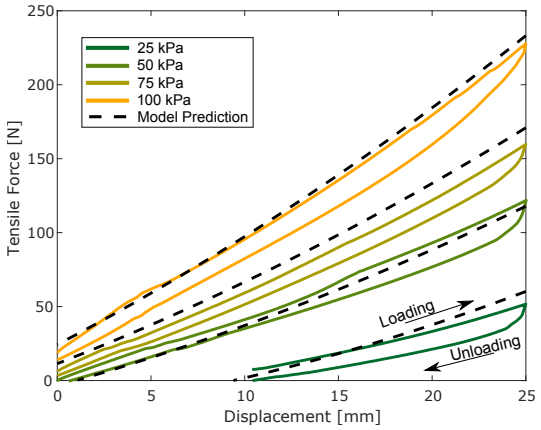

Fig. 4. Mean force-displacement curves of the SJBAM as a muscle from cyclic loading at 25, 50, 75, and 100 kPa.

2) Model Validation: Fig. 4 shows the mean SJBAM force-displacement curves and corresponding standard deviations as well as the theoretical SJBAM force-displacement curves. To obtain the tuning parameters for (16), we performed quasi-static cyclic loading tests on a standalone McKibben muscle. We follow the procedure outlined by Meller et al. [33] and determine tuning parameters using low-order polynomial fits.

The mean absolute percentage error between the experimental and simulation loading curves is 4.4% on average across the 20 trials. The results show that the brake can be made fairly transparent to the overall SJBAM while in loading and provide the additional benefit of increasing output contraction force compared to a traditional McKibben muscle.

Fig. 4 also shows that the tested SJBAM, which was based on a McKibben muscle, experiences hysteresis with loading/unloading as is typical of McKibben-type muscles. In a traditional McKibben muscle, Coulomb friction interactions between muscle components, such as the elastomeric bladder and fibers, produce motion history and result in force output differences for a given pressure and position. To quantify the increase in friction, the maximum hysteresis for an SJBAM as a muscle and a McKibben muscle were calculated for each of the four pressures tested. The average maximum hysteresis

Citation information: DOI 10.1109/TMECH.2022.3183576, IEEE Transactions on Mechatronics

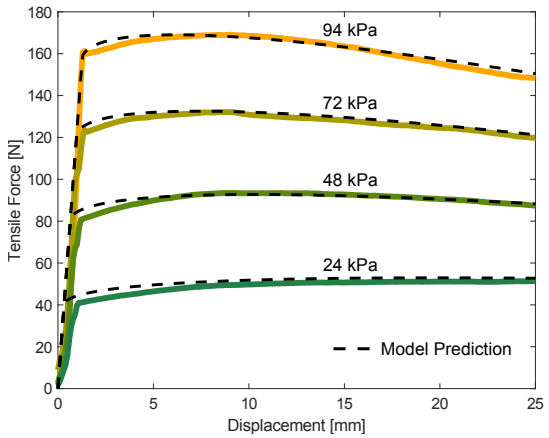

Fig. 5. Force-displacement curves of the SJBAM as a brake from tensile tests at four different ΔP, each listed above their corresponding loading curve.

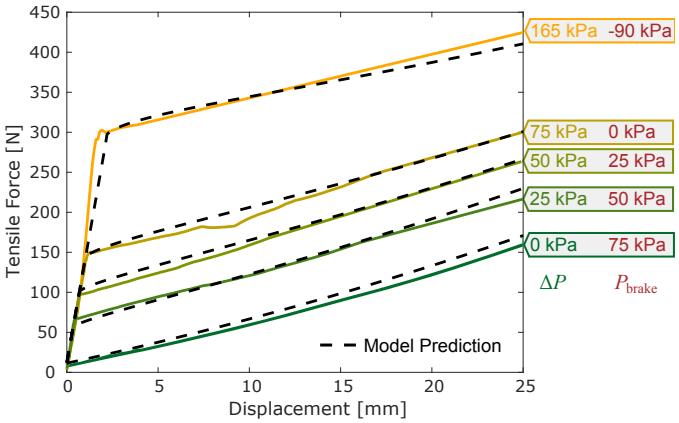

Fig. 6. Force-displacement curves of SJBAM with the muscle and brake active simultaneously. The muscle was set to 75 kPa and brake pressure was varied to produce desired ΔP.

across the tested pressures is 8% and 11% full-scale output for the McKibben muscle and SJBAM, respectively. This increase in hysteresis is likely due to the Coulomb friction between the brake layers. Because these layers can contact each other during the unjammed state, sliding of the brake layers can produce stick-slip, resulting in hysteresis. The silicone brake membrane's viscoelasticity could also contribute to hysteresis.

C. SJBAM as a Brake

To validate the SJBAM brake model, we performed quasi-static loading tests under isobaric conditions, with the SJBAM lengthened at 1 mm/s up to a 25 mm displacement from its minimum length. To operate an SJBAM solely as a brake, the muscle pressure P_o is set to atmospheric pressure while the brake pressure P_i is set below atmospheric pressure. We recorded force-displacement curves at four different pressures, in roughly 24 kPa increments.

We simulated the brake dynamic model in MATLAB (MathWorks) using kinetic friction coefficients for the entire motion. We used the PTFE-PTFE and PTFE-silicone friction coefficients measured by Choi et al. [31].

Fig. 5 shows the mean force-displacement curves for the layer jamming brake as well as the theoretical brake loading curves. The mean absolute percentage error between the experimental and simulation loading curves is 2.0% on average across all trials.

D. SJBAM Combined Muscle and Brake

When engaging the brake and muscle in the SJBAM simultaneously, we can either 1) maintain constant pressure in both the brake and the muscle or 2) vary the pressure, allowing for actively-tuned force-displacement curves during loading or unloading. We tested both conditions.

1) Constant Pressure: Fig. 6 shows the mean force-displacement curves and the simulated curves for an SJBAM with the muscle pressure $P_o = 75$ kPa and the brake pressure P_{brake} set at various pressures. Fig. 6 lists the pressure difference $\Delta P = P_o - P_{\text{brake}}$ producing each force-displacement curve as well as the corresponding absolute P_{brake}.

Here, we can see two novel properties of the SJBAM: 1) its use of positive-pressure layer jamming and 2) its super-atmospheric pressure range. Despite operating the brake above atmospheric pressure, because the McKibben muscle is at an even higher pressure, jamming still occurs. Therefore, even without a vacuum source, the brake of the SJBAM can still be used through this "positive-pressure" layer jamming. Furthermore, the properties of the brake can be actively controlled since we are able to directly control P_{brake}.

Because the brake operates inside of the higher pressure McKibben muscle, super-atmospheric pressure ranges are achievable, unlike with other jamming devices which are confined to a 1 atm pressure range due to operating in the atmosphere. The use of a vacuum produces additional brake force and allows for brake operation even at low McKibben pressures. In this case, a super-atmospheric ΔP of 165 kPa was achieved, resulting in over 125 N of additional braking force as compared to the $\Delta P = 100$ kPa case.

2) Tuned Force-Displacement Curves: The ability to independently vary the muscle and brake pressures allows the SJBAM to produce a range of forces at a given displacement. At a given displacement and PAM pressure, the minimum SJBAM force corresponds to the muscle force. The maximum SJBAM force is the sum of the forces produced by the muscle and the brake, where ΔP across the brake is maximized given the pressure sources available. The area between these bounding surfaces represents the range of achievable forces. Fig. 7(A) shows these bounds on SJBAM force when the atmosphere is the negative pressure source and $\Delta P_{\text{max}} = P_{\text{muscle}}$. A lower minimum pressure, such as vacuum, would further increase the maximum force, as Fig. 6 shows.

A McKibben muscle's displacement, pressure, and force are complexly coupled. In contrast, the relationship between SJBAM output force and brake pressure can simplify independent control of the SJBAM's force and displacement compared to that of a McKibben muscle.

We demonstrated the SJBAM's ability to actively tune its output force-displacement curve in an open-loop force control system. Fig. 7(C) shows the test set-up for these tuned force-displacement tests. One endcap of an SJBAM was mounted to

Citation information: DOI 10.1109/TMECH.2022.3183576, IEEE Transactions on Mechatronics

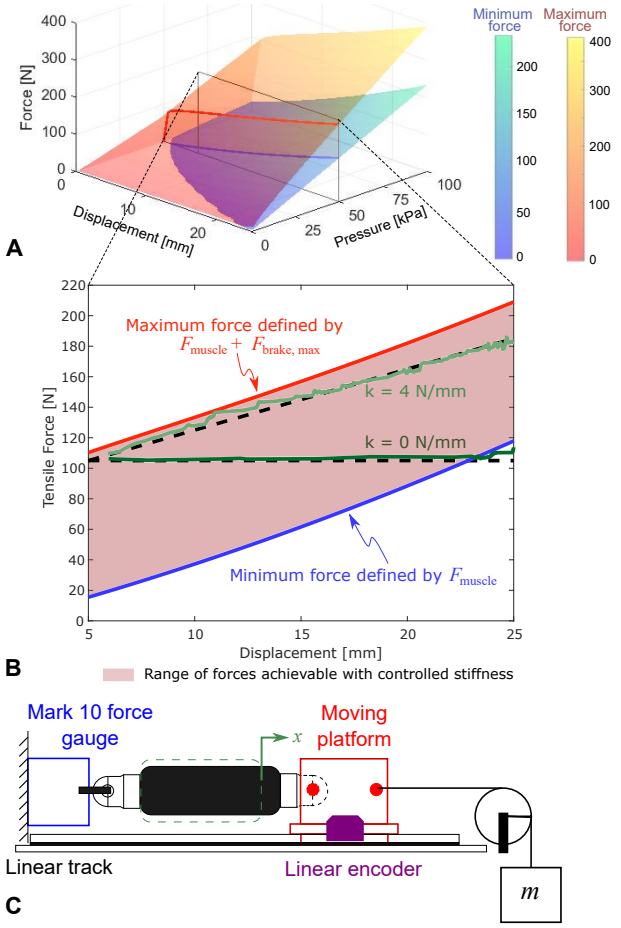

Fig. 7. By adjusting the brake pressure, the SJBAM can produce a range of forces for each muscle pressure. (A) The lower bound (in blue) is the minimum SJBAM force, corresponding to the muscle force. The upper bound (in red) is the combined muscle and max brake force. Bounds here are with the atmosphere as the negative pressure source. (B) For any given pressure, output force and displacement can be independently varied to yield desired force-displacement curves. (C) Test setup to measure force-displacement curves.

a Mark-10 force gauge while the other end cap was mounted to a moving platform on a linear track, allowing for 1-DOF movement. The displacement of the SJBAM was measured using a linear magnetic encoder (RLS LM15). Loads were applied to the SJBAM using weights connected via a pulley.

Using (15), we can derive the ΔP, and thus the P_{brake}, to achieve a desired stiffness. Fig. 7(B) shows two actively-tuned force displacement curves, with stiffnesses of 0 N/mm and 4 N/mm. The former shows the SJBAM's ability to render a constant force. Together, they are examples of the SJBAM's force control capabilities. Overall, any tuned force-displacement curve can be generated within the force bounds.

VI. Dynamic Experimental Results

A. Step Response

A limitation of McKibben muscles in dynamic applications is their relatively slow rise, fall, and delay times. Much of this stems from the time required to transfer the working fluid to/from the McKibben muscle volume.

By incorporating a brake into a PAM, the SJBAM reduces the volume needed to be pressurized. To examine the effects of this on the SJBAM's dynamic properties, the responses of an SJBAM and a standalone McKibben muscle to a step pressure increase and decrease of 100 kPa were recorded. Table I shows the 10-90% rise and fall times for the pressure inside each device as well as their 50% delay times. Across each of these parameters, the SJBAM as a muscle has improved dynamic response compared to the standalone McKibben muscle.

The SJBAM as a brake has a faster response than as a muscle, with lower rise, fall, and delay times due to the brake's smaller volume. This could allow the brake to quickly compensate for position errors in the muscle or act as a clutch, rapidly disengaging to allow for faster movement and then re-engaging to stop further muscle movement.

TABLE I
Step Response Times

	10-90% Rise	10-90% Fall	50% Rise Delay	50% Fall Delay
SJBAM as Brake	36.7 ms	151.5 ms	20.5 ms	80.8 ms
SJBAM as Muscle	130.9 ms	257.2 ms	173.0 ms	130.5 ms
McKibben Muscle	161.5 ms	263.9 ms	324.6 ms	196.2 ms

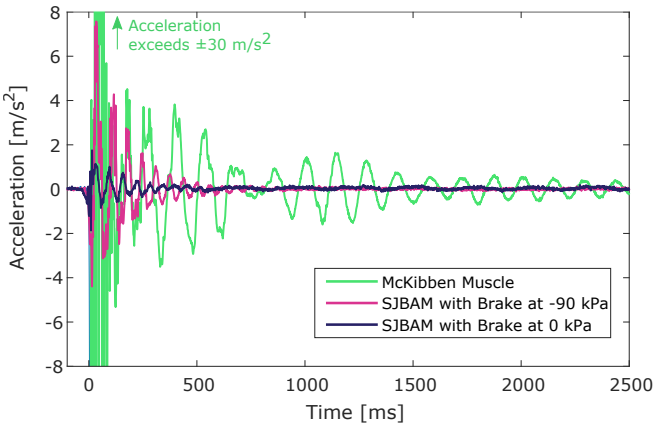

Fig. 8. Acceleration over time of free end cap following application of a dropped mass. Not only is peak acceleration amplitude much larger for the standalone McKibben muscle (reaching over 30 m/s^2), but oscillations continue for several seconds after they have been suppressed in the SJBAM.

B. Damping

We compare the stiffness change and damping capability of a McKibben muscle and of an SJBAM by measuring the acceleration resulting from an applied disturbance force. In these tests, one actuator end was clamped and the other suspended. A 2.5 kg mass was attached via a nylon rope to the free end. The mass was then lifted 5 mm above its equilibrium rest position and dropped. The resulting acceleration profile was recorded using an accelerometer mounted on the free end for three conditions: a standalone McKibben muscle, an SJBAM with $P_{\text{brake}} = 0$ kPa, and an SJBAM with $P_{\text{brake}} = -90$ kPa. All trials had a muscle pressure of 75 kPa.

Fig. 8 shows the response for the equivalent McKibben muscle. The McKibben muscle's relatively low stiffness results in high peak acceleration from the muscle's inability to dissipate the kinetic energy, and its low damping results in continued oscillation for several seconds.

Citation information: DOI 10.1109/TMECH.2022.3183576, IEEE Transactions on Mechatronics

Fig. 8 also shows the response for the SJBAM with the brake activated. In both cases with the brake engaged, the brake dissipates the kinetic energy, resulting in lower peak acceleration than with the McKibben muscle. Afterwards, the friction damping clamps the muscle position, preventing further oscillation. The energy dissipated is a function of brake pressure and displacement. The brake at 0 kPa dissipates more energy than at −90 kPa due to its ability to travel further. Given a known disturbance to reject, the pressure of the brake can be preset to absorb the largest amount of energy.

To achieve similar small deflections, a traditional McKibben muscle would need to be highly pressurized to increase its spring constant. However, this results mainly in storage of the impact energy, potentially resulting in rebound, and greatly increases the corresponding loading forces on the support structure. The use of the brake mitigates both these effects.

Even with a high internal pressure, a McKibben muscle has comparatively low damping, as evidenced by the long McKibben settling time in Fig. 8. This is disadvantageous for precise positioning without overshoot or maintaining a desired position in the face of external disturbances.

The SJBAM's brake acts as a friction damper, absorbing excess energy. The brake has a high stiffness below a certain force threshold, after which, its stiffness decreases dramatically. When the brake enters the latter region, it dissipates energy. This two-phase behavior is particularly advantageous for maintaining a desired position without excessively stressing the robot structure. By setting the pressure gradient across the brake, the force below which the SJBAM will minimally yield can be selected. However, upon encountering forces exceeding this threshold, the brake dissipates the excess energy. Thus, the SJBAM can be made very stiff but upon encountering dangerously high forces, will compliantly yield, dissipating excess energy and preventing structural damage.

VII. 1 Degree of Freedom Manipulator

One potential application for SJBAMs is in manipulators used in physical human-robot interaction. Therefore, we conducted demonstrations using a 1-DOF manipulator.

A. Setup Overview

Fig. 9 shows the 1-DOF manipulator with antagonistic PAMs – McKibben muscles or SJBAMs – used in our experiments. PAM contractile force is transmitted to the axis of rotation via a pulley. Angular displacement was recorded using a Bourns EMS22 rotary encoder. The manipulator was mounted parallel to the ground to avoid gravitational effects.

Fig. 10 illustrates three operating modes of the SJBAM: as a brake, a muscle, or a hybrid mode in which the muscle and brake are both active. These modes can be used for energy storage or its release. In the muscle mode, the SJBAM behaves like a McKibben muscle, enabling the storage and release of elastic energy like other passively compliant actuators. In the brake mode, the SJBAM can act as a friction-based clutch which locks the displacement of the SJBAM without consuming energy while clutching. In the hybrid mode, the SJBAM acts as a clutch with enhanced locking force but with a slower response time compared to the standalone brake mode due to the need to repressurize to a higher pressure.

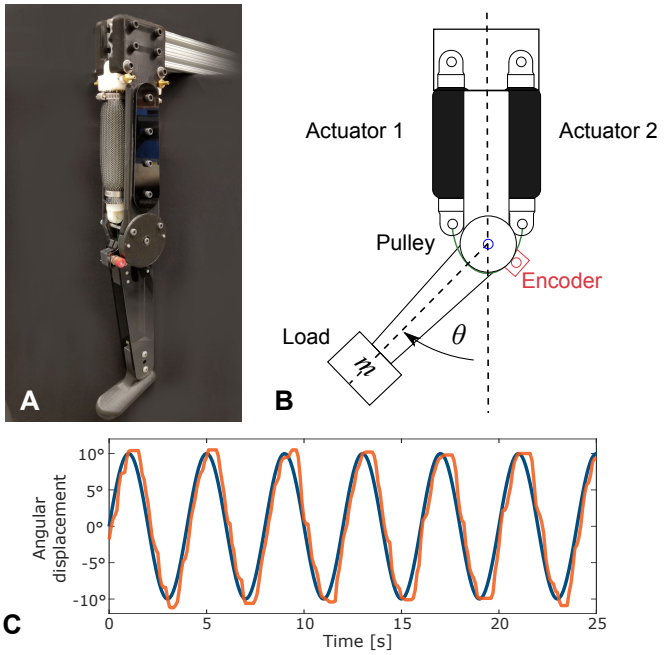

Fig. 9. 1-DOF manipulator setup. (A) Photo of 1-DOF manipulator used in experimental setup. For testing, this manipulator was mounted parallel to the ground to avoid gravitational effects. (B) Top-down schematic of 1-DOF manipulator. The actuators used can be either McKibben muscles or SJBAMs. (C) Position tracking: reference in dark blue and measured position in orange

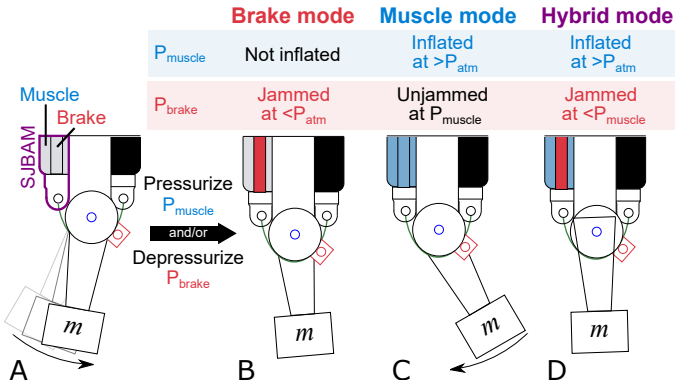

Fig. 10. The SJBAM, shown as the left actuator in each subfigure, can function in three primary modes. (A) The SJBAM can either store or dissipate energy following acceleration of the manipulator. (B) In brake mode, the jammed brake dissipates energy through friction. (C) In muscle mode, the SJBAM functions like a McKibben muscle and can store energy for rebound. (D) In hybrid mode, both the brake and muscle are active.

The brake and hybrid modes can also be used for energy dissipation. In these modes, the jamming brake can passively dissipate energy. With the hybrid mode in particular, this can allow for tuning of the amount of energy to be stored in the muscle and the amount to be dissipated through the brake.

B. Demonstrations

1) Dynamic Braking: We demonstrated the SJBAM in a dynamic braking application using the 1-DOF manipulator setup. We compared the braking performance of the SJBAM

Citation information: DOI 10.1109/TMECH.2022.3183576, IEEE Transactions on Mechatronics

and a McKibben muscle using the 1-DOF manipulator with a bang-bang controller. For the McKibben muscle, it was repressurized to 75 kPa to actively drive the end effector back to its starting position. For the SJBAM, after crossing the desired angular position, the brake pressure was set to vacuum.

The McKibben muscle took 264 ms to return to the desired position after initially crossing it, featured a maximum overshoot of 11.4°, and the bang-bang control results in continued oscillation. The SJBAM settling time was 257 ms with a maximum overshoot of 4.95°; the system settled at 0.6° from the desired position. Thus, the SJBAM achieves quick, stable deceleration using a simple control strategy.

2) Closed-Loop Position Tracking: We demonstrated closed-loop position tracking for a 0.25 Hz sinusoid with 10° amplitude using a 1-DOF manipulator with antagonistic SJBAMs. For this proof of concept, a proportional controller controlled the muscle pressure. A bang-bang controller controlled the brake pressure, with the brake being toggled between being unjammed when the end effector position was within $\pm 10°$ and jammed otherwise to reduce overshoot. Fig. 9(C) shows the results of this test, with an average peak overshoot of 0.39°. More robust closed-loop position control is an area for future work, as discussed in Sec. VIII.

VIII. Discussion

The SJBAM expands the capabilities of PAMs and jamming devices in a compact, compliant package. Compared to a traditional McKibben actuator, the SJBAM has higher force output, faster dynamic response, enhanced damping, and independent position and stiffness control. Compared to a traditional jamming device, the SJBAM enables super-atmospheric pressure ranges and positive-pressure layer jamming.

The SJBAM mirrors biological muscle in many respects. Biological muscle is also a modal actuator, acting like a unidirectional motor while shortening, performing positive net work, and like a controllable variable brake while lengthening, resisting a change in length under load [1]. This originates from the structure of myosin filaments in muscle fibers which have two motor domains – one which acts as a motor and the other as a fast-acting brake when the muscle is stretched [34].

The SJBAM concept itself is more general than the implementation presented which incorporated a layer jamming brake inside of a contractile-type pneumatic McKibben muscle. The general concept can be extended to other PAMs with strains less than 100%. The SJBAM inherits some limitations from its constituent parts which could be addressed through using different actuators or brake designs while retaining the more fundamental benefits stemming from incorporating a brake inside of a fluidic muscle. Embedding the jamming brake in a PAM with lower hysteresis, more linearity, and lower deadband pressure than a McKibben muscle, like a pleated PAM, would directly improve those properties in the SJBAM.

Just as with the layer jamming brake, the SJBAM performs best in tension due to possible buckling of the brake layers.

Stiffening the layers, through increasing thickness or using materials with a higher elastic modulus, could address this. Additionally, an alternative jamming brake design or geometry such as fiber jamming could potentially be used.

In general, the use of a jamming brake in a hybrid mode for the SJBAM will result in a trade-off between certain enhanced capabilities, such as more precise position control, and reduced energy efficiency due to energy loss via friction.

One area of future work is more robust closed-loop position control. Building on the preliminary results shown in Sec. VII-B2, a phase plane switching controller embedded within a larger PID position control loop could be used for a 1-DOF manipulator. The SJBAM's quicker dynamic response, energy dissipation, and stiffening can enable more aggressive control compared to McKibben muscles, while reducing overshoot and underdamped behavior. Because the SJBAM's brake operates best generating torque opposing the direction of motion, a phase plane switching controller can be used where the brake opposing the joint motion is activated to adjust position and the other brake is set to its corresponding muscle pressure, resulting in no jamming in that brake. Braking torque is thus:

$$\tau_b = \tau_{b1} + \tau_{b2} \tag{17}$$

where one of τ_{b1} or $\tau_{b2} = 0$ at any given time. This generated torque is not velocity-dependent [31]. This control strategy could be adapted for torque control and incorporate pressure and system dynamics. Additional behavior, such as using an opposing brake as a clutch, could also be incorporated.

IX. Conclusions

In this paper, we presented the concept for the SJBAM, a hybrid artificial muscle with an embedded layer jamming brake. This combination produced an all-soft VIA with synergistic properties: 1) super-atmospheric and positive pressure jamming for the brake, 2) increased muscle force production, and 3) faster dynamic response.

We derived quasi-static models for the SJBAM's operating modes and its stiffness. We conducted quasi-static experiments verifying these models and dynamic experiments investigating the dynamic response to a step pressure input and an external disturbance. We showed that the SJBAM also possesses new abilities like direct stiffness control, enhanced damping, and demonstrated its use in a 1-DOF manipulator. Future work includes further investigation of closed-loop position and stiffness control of the SJBAM in arrangements like a 1-DOF manipulator to translate the SJBAM to real-world applications.

References

[1] M. H. Dickinson, C. T. Farley, R. J. Full, M. A. R. Koehl, R. Kram, and S. Lehman, "How animals move: An integrative view," *Science*, vol. 288, no. 5463, pp. 100–106, 2000.

[2] Z. Shen and J. Seipel, "A fundamental mechanism of legged locomotion with hip torque and leg damping," *Bioinspiration & biomimetics*, vol. 7, no. 4, p. 046010, 2012.

[3] T. A. McMahon and G. C. Cheng, "The mechanics of running: How does stiffness couple with speed?" *Journal of Biomechanics*, vol. 23, pp. 65 – 78, 1990, International Society of Biomechanics.

[4] B. Vanderborght, A. Albu-Schaeffer, A. Bicchi, E. Burdet, D. G. Caldwell, R. Carloni, M. Catalano, O. Eiberger, W. Friedl, G. Ganesh, M. Garabini, M. Grebenstein, G. Grioli, S. Haddadin, H. Hoppner, A. Jafari, M. Laffranchi, D. Lefeber, F. Petit, S. Stramigioli, N. Tsagarakis, M. Van Damme, R. Van Ham, L. C. Visser, and S. Wolf, "Variable impedance actuators: A review," *Robotics and Autonomous Systems*, vol. 61, no. 12, pp. 1601–1614, 2013.

[5] M. Laffranchi, L. Chen, N. Kashiri, J. Lee, N. G. Tsagarakis, and D. G. Caldwell, "Development and control of a series elastic actuator equipped with a semi active friction damper for human friendly robots," *Robotics and Autonomous Systems*, vol. 62, no. 12, pp. 1827–1836, 2014.

[6] S. Haddadin, A. Albu-Schäffer, O. Eiberger, and G. Hirzinger, "New insights concerning intrinsic joint elasticity for safety," in *IEEE/RSJ International Conference on Intelligent Robots and Systems*, 2010, pp. 2181–2187.

[7] N. Kashiri, G. A. Medrano-Cerda, N. G. Tsagarakis, M. Laffranchi, and D. Caldwell, "Damping control of variable damping compliant actuators," in *2015 IEEE International Conference on Robotics and Automation (ICRA)*, 2015, pp. 850–856.

[8] D. Rus and M. T. Tolley, "Design, fabrication and control of soft robots," *Nature*, vol. 521, no. 7553, pp. 467–475, 2015.

[9] D. Shin, X. Yeh, and O. Khatib, "A new hybrid actuation scheme with artificial pneumatic muscles and a magnetic particle brake for safe human-robot collaboration," *International Journal of Robotics Research*, vol. 33, no. 4, pp. 507–518, 2014.

[10] M. Manti, V. Cacucciolo, and M. Cianchetti, "Stiffening in soft robotics: A review of the state of the art," *IEEE Robotics & Automation Magazine*, vol. 23, no. 3, pp. 93–106, 2016.

[11] B. Tondu, "Modelling of the McKibben artificial muscle: A review," *Journal of Intelligent Material Systems and Structures*, vol. 23, no. 3, pp. 225–253, 2012.

[12] F. Daerden and D. Lefeber, "Pneumatic artificial muscles: actuators for robotics and automation," *European Journal of Mechanical and Environmental Engineering*, vol. 47, pp. 10–21, 2000.

[13] C. P. Chou and B. Hannaford, "Measurement and modeling of McKibben pneumatic artificial muscles," *IEEE Transactions on Robotics and Automation*, vol. 12, no. 1, pp. 90–102, 1996.

[14] R. Van Ham, T. G. Sugar, B. Vanderborght, K. W. Hollander, and D. Lefeber, "Compliant actuator designs," *IEEE Robotics & Automation Magazine*, vol. 16, no. 3, pp. 81–94, 2009.

[15] L. A. Al Abeach, S. Nefti-Meziani, and S. Davis, "Design of a variable stiffness soft dexterous gripper," *Soft Robotics*, vol. 4, no. 3, pp. 274–284, 2017.

[16] C. Xiang, M. E. Giannaccini, T. Theodoridis, L. Hao, S. Nefti-Meziani, and S. Davis, "Variable stiffness McKibben muscles with hydraulic and pneumatic operating modes," *Advanced Robotics*, vol. 30, no. 13, pp. 889–899, 2016.

[17] A. Shiva, A. Stilli, Y. Noh, A. Faragasso, I. De Falco, G. Gerboni, M. Cianchetti, A. Menciassi, K. Althoefer, and H. A. Wurdemann, "Tendon-based stiffening for a pneumatically actuated soft manipulator," *IEEE Robotics and Automation Letters*, vol. 1, no. 2, pp. 632–637, 2016.

[18] G. K. Klute, J. M. Czerniecki, and B. Hannaford, "Artificial muscles: Actuators for biorobotic systems," *The International Journal of Robotics Research*, vol. 21, no. 4, pp. 295–309, 2002.

[19] E. D. Tytell, J. A. Carr, N. Danos, C. Wagenbach, C. M. Sullivan, T. Kiemel, N. J. Cowan, and M. M. Ankarali, "Body stiffness and damping depend sensitively on the timing of muscle activation in lampreys," *Integrative and Comparative Biology*, vol. 58, no. 5, pp. 860–873, 2018.

[20] S. Heitmann, M. Breakspear, and N. Ferns, "Muscle co-contraction modulates damping and joint stability in a three-link biomechanical limb," *Frontiers in Neurorobotics*, vol. 5, p. 5, 2012.

[21] T. D. C. Thanh and K. K. Ahn, "Intelligent phase plane switching control of pneumatic artificial muscle manipulators with magneto-rheological brake," *Mechatronics*, vol. 16, no. 2, pp. 85 – 95, 2006.

[22] T. Noritsugu, Y. Tsuji, and K. Ito, "Improvement of control performance of pneumatic rubber artificial muscle manipulator by using electrorheological fluid damper," in *IEEE International Conference on Systems, Man, and Cybernetics*, vol. 4. IEEE, 1999, pp. 788–793.

[23] S. Follmer, D. Leithinger, A. Olwal, N. Cheng, and H. Ishii, "Jamming User Interfaces: Programmable Particle Stiffness and Sensing for Malleable and Shape-Changing Devices," *ACM Symposium on User Interface Software and Technology*, pp. 519–528, 2012.

[24] J. R. Amend, E. Brown, N. Rodenberg, H. M. Jaeger, and H. Lipson, "A positive pressure universal gripper based on the jamming of granular material," *IEEE Transactions on Robotics*, vol. 28, no. 2, pp. 341–350, 2012.

[25] A. Jiang, G. Xynogalas, P. Dasgupta, K. Althoefer, and T. Nanayakkara, "Design of a variable stiffness flexible manipulator with composite granular jamming and membrane coupling," in *IEEE/RSJ International Conference on Intelligent Robots and Systems*, 2012, pp. 2922–2927.

[26] Y. J. Kim, S. Cheng, S. Kim, and K. Iagnemma, "A novel layer jamming mechanism with tunable stiffness capability for minimally invasive surgery," *IEEE Transactions on Robotics*, vol. 29, no. 4, pp. 1031–1042, 2013.

[27] V. Wall, R. Deimel, and O. Brock, "Selective stiffening of soft actuators based on jamming," in *IEEE International Conference on Robotics and Automation*, 2015, pp. 252–257.

[28] Y. Li, Y. Chen, Y. Yang, and Y. Wei, "Passive Particle Jamming and Its Stiffening of Soft Robotic Grippers," *IEEE Transactions on Robotics*, vol. 33, no. 2, pp. 446–455, 2017.

[29] C. Mikol and H. Su, "An actively controlled variable stiffness structure via layer jamming and pneumatic actuation," in *International Conference on Robotics and Automation*, 2019, pp. 7555–7561.

[30] Y. S. Narang, A. Degirmenci, J. J. Vlassak, and R. D. Howe, "Transforming the dynamic response of robotic structures and systems through laminar jamming," *IEEE Robotics and Automation Letters*, vol. 3, no. 2, pp. 688–695, 2018.

[31] I. Choi, N. Corson, L. Peiros, E. W. Hawkes, S. Keller, and S. Follmer, "A soft, controllable, high force density linear brake utilizing layer jamming," *IEEE Robotics and Automation Letters*, vol. 3, no. 1, pp. 450–457, 2018.

[32] R. W. Colbrunn, G. M. Nelson, and R. D. Quinn, "Modeling of braided pneumatic actuators for robotic control," in *IEEE/RSJ International Conference on Intelligent Robots and Systems*, vol. 4, 2001, pp. 1964–1970 vol.4.

[33] M. A. Meller, M. Bryant, and E. Garcia, "Reconsidering the McKibben muscle: Energetics, operating fluid, and bladder material," *Journal of Intelligent Material Systems and Structures*, vol. 25, no. 18, pp. 2276–2293, 2014.

[34] E. Brunello, M. Reconditi, R. Elangovan, M. Linari, Y.-B. Sun, T. Narayanan, P. Panine, G. Piazzesi, M. Irving, and V. Lombardi, "Skeletal muscle resists stretch by rapid binding of the second motor domain of myosin to actin," *Proceedings of the National Academy of Sciences*, vol. 104, no. 50, pp. 20 114–20 119, 2007.

Brian H. Do received his M.S. degree in mechanical engineering from Stanford University in 2019, where he is currently working towards the Ph.D. degree. He received his B.S. degree in mechanical engineering from the Georgia Institute of Technology in 2017. His research interests include soft robotics, variable stiffness structures, and compliant mechanisms.

Inrak Choi received his PhD degree in mechanical engineering from Stanford University in 2019. His research has focused on novel actuation and mechanisms for physical human-robot interfaces. He is now a postdoctoral research fellow at Seoul National University for military service in South Korea.

Sean Follmer is an Assistant Professor of mechanical engineering and computer science (by courtesy) at Stanford University, Stanford, CA, USA. Dr. Follmer directs the Stanford Shape Lab and is a member of the Stanford HCI Group. Dr. Follmer received a PhD and a Masters from the MIT Media Lab in 2015 and 2011 (respectively) for his work in human-computer interaction, and a BS in Engineering with a focus on Product Design from Stanford University.